Available online at www.sciencedirect.com
SCIENCE DIRECT®
Tectonophysics 378 (2004) 165–181
TECTONOPHYSICS
www.elsevier.com/locate/tecto

Textural evidence for recent co-seismic circulation of fluids in the Nojima fault zone, Awaji island, Japan

Anne-Marie Boullier[a,*], Koichiro Fujimoto[b], Tomoyuki Ohtani[b], Gabriela Roman-Ross[a], Éric Lewin[c], Hisao Ito[b], Philippe Pezard[d], Benoît Ildefonse[d]

[a] *LGIT (CNRS), UMR 5559, Université Joseph Fourier, BP 53, 38041 Grenoble, France*
[b] *Geological Survey of Japan, AIST, Central 7, 1-1-1, Higashi, Tsukuba, Ibaraki 305-8567, Japan*
[c] *LGCA (CNRS), UMR 5559, Université Joseph Fourier, BP 53, 38041 Grenoble, France*
[d] *Laboratoire de Tectonophysique, ISTEEM, Université Montpellier II, 34095 Montpellier cedex 05, France*

Accepted 11 September 2003

Abstract

The Hirabayashi borehole (Awaji Island, Japan) was drilled by the Geological Survey of Japan (GSJ) 1 year after the Hyogo-ken Nanbu (Kobe) earthquake (1995, $M_{JMA}=7.2$). This has enabled scientists to study the complete sequence of deformation across the active Nojima fault, from undeformed granodiorite to the fault core. In the fault core, different types of gouge and fractures have been observed and can be interpreted in terms of a complex history of faulting and fluid circulation. Above the fault core and within the hanging wall, compacted cataclasites and gouge are cut by fractures which show high apparent porosity and are filled by 5–50 μm euhedral and zoned siderite and ankerite crystals. These carbonate-filled fractures have been observed within a 5.5-m-wide zone above the fault, but are especially abundant in the vicinity (1 m) of the fault. The log-normal crystal size distributions of the siderite and ankerite suggest that they originated by decaying-rate nucleation accompanied by surface-controlled growth in a fluid saturated with respect to these carbonates. These carbonate-filled fractures are interpreted as the result of co-seismic hydraulic fracturing and upward circulation of fluids in the hanging wall of the fault, with the fast nucleation of carbonates attributed to a sudden fluid or CO_2 partial pressure drop due to fracturing. The fractures cut almost all visible structures at a thin section scale, although in some places, the original idiomorphic shape of carbonates is modified by a pressure-solution mechanism or the carbonate-filled fractures are cut and brecciated by very thin gouge zones; these features are attributed to low and high strain-rate mechanisms, respectively. The composition of the present-day groundwater is at near equilibrium or slightly oversaturated with respect to the siderite, calcite, dolomite and rhodochrosite. Taken together, this suggests that these fractures formed very late in the evolution of the fault zone, and may be induced by co-seismic hydraulic fracturing and circulation of a fluid with a similar composition to the present-day groundwater. They are therefore potentially related to recent earthquake activity (<1.2 Ma) on the Nojima fault.
Published by Elsevier B.V.

Keywords: Active fault; Co-seismic hydraulic fracturing; Fluid circulation; Carbonate infilling

* Corresponding author. Fax: +33-4-7682-8101.
E-mail address: Anne-Marie.Boullier@obs.ujf-grenoble.fr (A.-M. Boullier).

0040-1951/$ - see front matter. Published by Elsevier B.V.
doi:10.1016/j.tecto.2003.09.006

1. Introduction

The role of fluid pressure in faulting processes has been recognised for a long time (Secor, 1965). A more recent status of our knowledge of involvement of fluids in the seismic cycle has been summarised by Hickman et al. (1995). At depth, hydrothermal veining or cemented fault breccias are good evidence for fluid circulation and seismic activity within or above the seismogenic zone (Sibson et al., 1988; Cox, 1995; Robert et al., 1995; Sibson and Scott, 1998; Eichhubl and Boles, 2000; de Ronde et al., 2001). At the surface level, hydrological changes occur after major earthquakes and are dependent on the style of faulting (Muir-Wood and King, 1993). Tsunogai and Wakita (1995) have reported chemical variations in ground water composition just before the Hyogo-ken Nanbu (Kobe) earthquake in Japan. Fluid flow through the crust may be, therefore, seismically influenced and faults may play an important role in redistributing fluids in the shallow crust.

Boreholes through active faults offer a good opportunity to study both structures and physical characteristics of faults zones, especially their fluid flow properties. In order to better understand the relationships between recent faulting and fluid transfer along the active Nojima fault (Japan), the youngest carbonate-filled fractures observed in the Hirabayashi drill core samples have been studied in detail. In this paper, we present the geometry and internal structures of these carbonate-filled fractures, compare the chemical composition of their filling minerals with that of the borehole groundwater, and attempt to interpret them in terms of recent co-seismic fracturing and redistribution of fluids in the fault zone.

2. Geological setting

The 1995 Hyogo-ken Nanbu (Kobe) earthquake (M_{JMA}=7.2, M_W=6.9) produced a 10.5-km-long surface rupture with reverse dextral slip along the Nojima fault on the northwest coast of Awaji Island, south of Kobe (Awata and Mizuno, 1997). A total of 490–540 m vertical offset of the Kobe Group unconformity in contact with Cretaceous granodiorite and porphyry dikes (Fig. 1) has occurred during the last 1.2 My (Murata et al., 2001).

In 1996, the Geological Survey of Japan drilled a 746.7-m subvertical borehole which encountered the 85° southeastward-dipping fault at 625 m depth (Fig. 1). Conventional geophysical logging (electrical resistivity and natural gamma radioactivity) and other logging tools were used in order to allow a complete characterization of the borehole (Ito et al., 1996). Drill cores were recovered corresponding to almost the entire depth interval from 150.2 to 746.7 m within Cretaceous granodiorite and porphyry dikes (Fig. 1). The petrography, mineralogy (primary and alteration assemblages) and structures along the whole borehole have been described by Ito et al. (1996), Tanaka et al. (2001), Fujimoto et al. (2001), and Ohtani et al. (2000, 2001). The fault architecture has been defined by Ohtani et al. (2000) on the basis of alteration and deformation features. Following the terminology proposed by Caine et al. (1996), a fault core characterized by gouges and cataclasites was intersected at the depth range of 623.1–625.3 m. Considering the relative orientation of the fault and borehole, the fault core is 0.3 m thick in a direction normal to the fault. The damage zone, defined by small faults, breccias, veins and alteration minerals, was encountered between 426.2 m and the bottom of the borehole (746.7 m).

The fault zone has undergone a complex history as shown by various superimposed structures in the samples. For example, fluid inclusions hosted by pseudotachylytes in the fault core show that these rocks have been formed at around 15 km depth during large seismic events and have been subsequently uplifted to 625 m below the present-day surface (Boullier et al., 2001). This uplift occurred before the deposition of the Iwaya Formation at the base of the Kobe Group, which is middle to late Eocene in age (Yamamoto et al., 2000).

Three stages of hydrothermal alteration are reported by Ohtani et al. (2000) on the basis of mineral assemblages and fluid inclusions: chloritization at temperature higher than 200 °C, zeolite mineralization at temperature lower than 200 °C, and carbonate mineralization related to recent fluid flow. In this paper, we will focus on this third stage, and in particular, on the latest carbonate veins which cut almost all the previous structures. These veins are filled by numerous idiomorphic, carbonate rhombs (ankerite and siderite), a rare internal texture which has only been described previously in a few instances

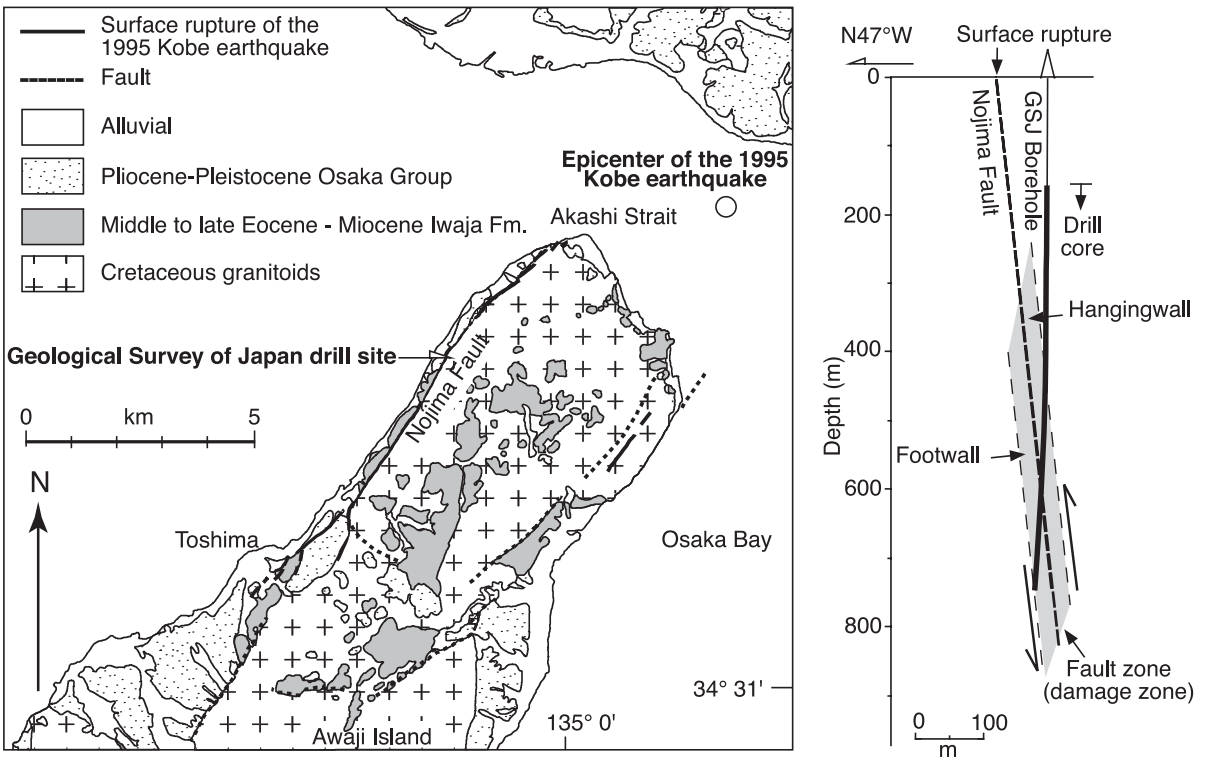

Fig. 1. Geological map of Awaji Island and sketch of the Hirabayashi borehole showing the relative orientations of the fault and borehole. The shaded pattern represents the fault zone (i.e. damage zone). G.S.J.: Geological Survey of Japan.

(see the review by Bons, 2000), and which may have important significance for fluid circulation related to seismic processes.

3. Description of structures

The carbonate veins have been studied at three different scales: on a macroscopic scale of polished slabs from the drill core samples, on a thin section scale with a petrographical microscope, and on a microscopic scale using a scanning electron microscope (SEM).

3.1. Macrostructures

Polished slabs from the drill core samples were studied from a depth interval between 553.39 and 718.20 m, and the results compared to data available from thin sections. Two types of fine-grained carbonate veins are distinguished at the macroscopic scale: (1) orange to red-brown carbonate veins (Fig. 2a), and (2) light brown to beige late carbonate veins (Fig. 2 b to f). The two types of veins generally cut breccias, compacted cataclasites and gouges (Fig. 2). They are generally orientated at high angles to the schistosity, but they may also be locally parallel to it, resulting in an irregular saw-tooth aspect to the fractures (Figs. 2e,f and 3). In some places, the fine-grained carbonate crystals constitute the cement of breccias and fill the voids between the clasts (Fig. 2c). The maximum thickness of the veins, as seen on the polished slabs, is 1–2 cm (see Fig. 2b).

3.2. Microstructures

3.2.1. Ankerite–siderite veins

The fractures have irregular shapes and sharp walls which may be fitted together as in a jigsaw

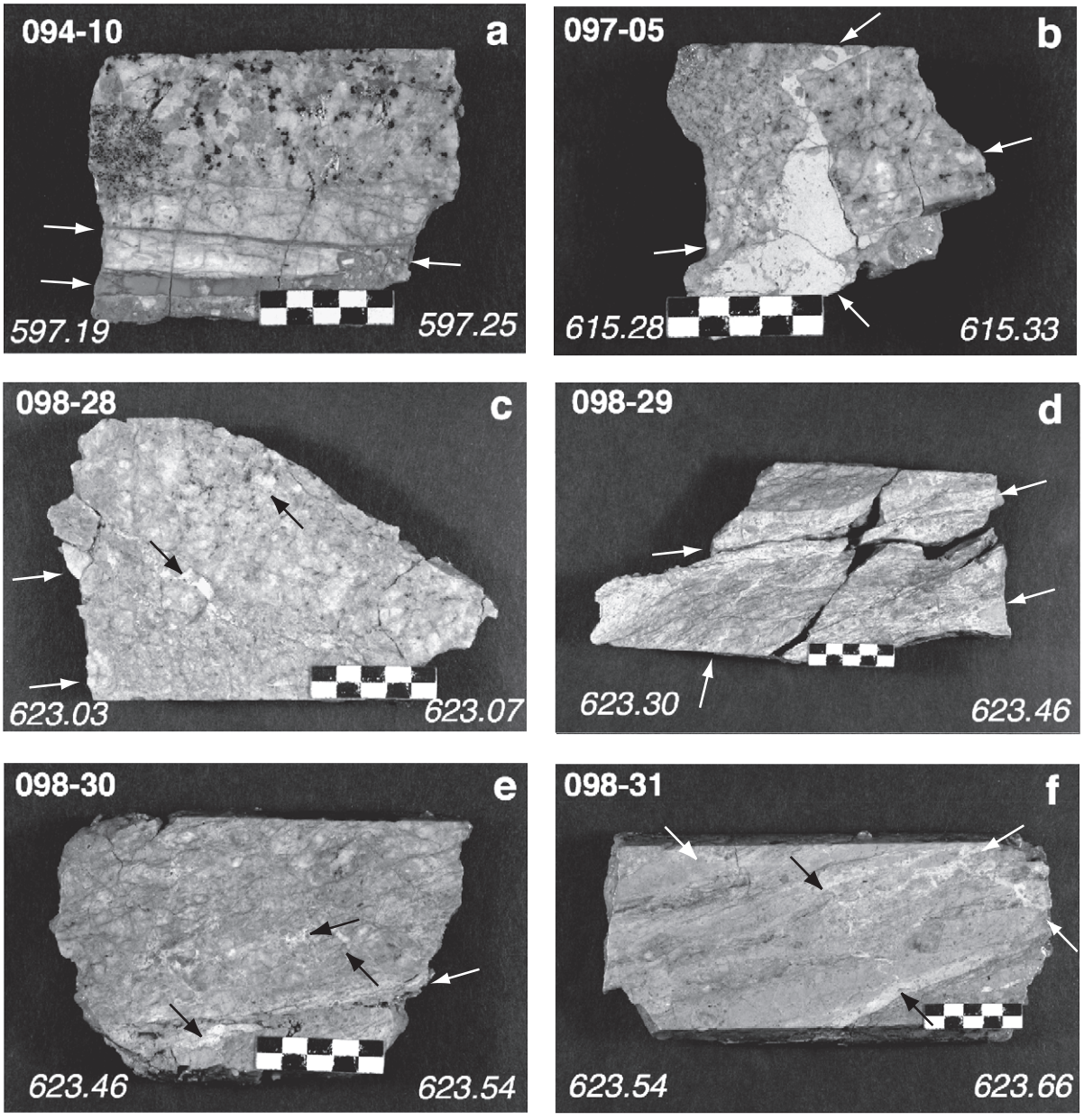

Fig. 2. Photographs of polished drill core slabs. The depths of the upper and lower limits of the samples are specified in italics at the bottom of each image (top always on the left side). The sample number (upper left corner) indicates the number of the drill core box and the number of the sample within that box. Siderite±ankerite filled fractures are shown by white or black arrows. The scale marker is 2.5 cm long.

puzzle (Fig. 3). Near the fault core, the light brown to beige carbonate infill is composed of numerous siderite and ankerite rhombs, and the veins cut structures such as compacted gouges or cataclasites, blocky zeolite (laumontite) or calcite veins, and thin siderite veinlets which are parallel to the schistosity

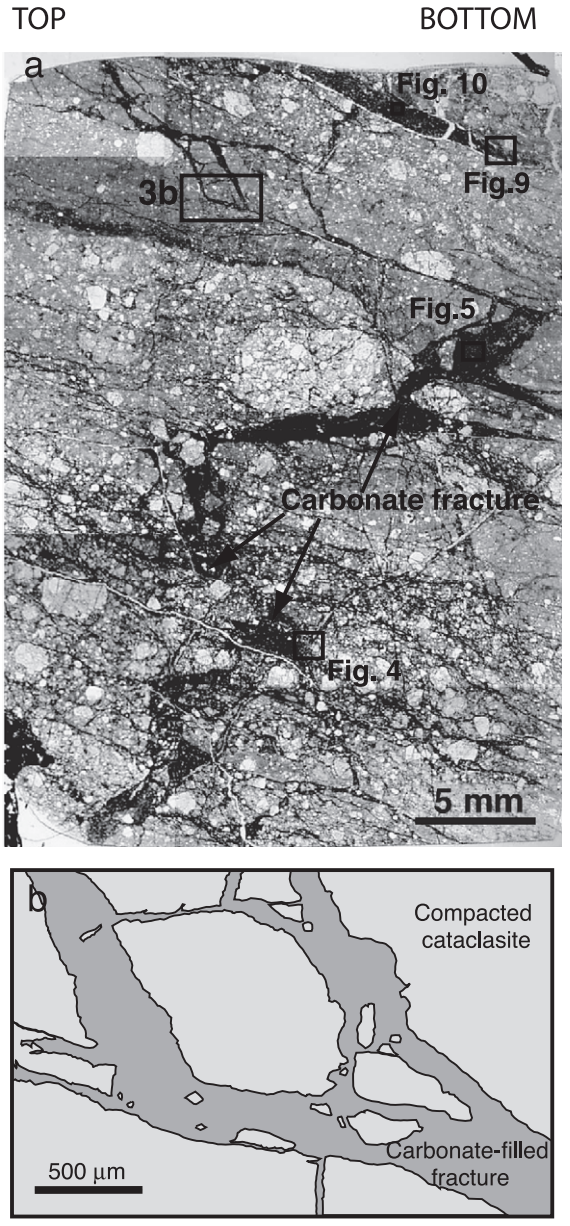

Fig. 3. (a) Photograph of thin section HR2-48 taken from slab 098-31 slab (see Fig. 2f); (b) sketch of the detail area outlined by box (b). Note the saw-tooth shape of the carbonate-filled fractures which appear dark in the photograph. Locations of Figs. 4, 5, 9 and 10 are also shown.

(Fig. 4). All of these components from the host rocks may be incorporated as fragments into the fractures and cemented by small siderite and ankerite crystals. The small siderite rhombs (7.1 ∅ μm average) often form inclusions in the larger crystals of ankerite (15.9 ∅ μm average); the reverse relationship has not been observed. The minimum thickness of fractures is less than 10 μm, which corresponds to the average size of a single rhomb of siderite. Numerous voids remain between the rhombs suggesting a high overall porosity of the fracture infill (Fig. 5).

Siderite and ankerite rhombs are locally found in variable proportions within a single fracture (Fig. 5). The siderite crystals are apparently homogeneous in composition or slightly zoned, as they appear darker in the centre when observed in back-scattered electron mode on a scanning electron microscope (BSE-SEM). The ankerite crystals display a very fine oscillatory zoning, which in general corresponds to a slightly darker rim visible on BSE-SEM images (Figs. 5 and 6).

In order to understand the crystallization processes of the siderite and ankerite minerals (Kile et al., 2000), the long diagonals crystals were manually measured on SEM images (Fig. 5) using the public domain NIH image program (developed at the U.S. National Institutes of Health and available on the Internet at http://rsb.info.nih.gov/nih-image/). More than 300 crystals were measured for each type of carbonate on isolated crystals; siderite crystals forming inclusions within ankerite were avoided. Both sets of measurements follow log-normal distributions with a good approximation (Fig. 7). Both distributions display similar shapes (same standard deviation over mean value ratio).

3.2.2. Siderite veins

At 597.19 m depth, i.e. at 2.8 m away from the fault plane within the hanging wall, the orange to red-brown carbonate fractures (Fig. 2a) display different internal structures. The carbonate veins are filled with fragments of the altered wall rock and by small siderite crystals which appear to fill almost all the voids. Thus, the apparent porosity is much lower than in the siderite–ankerite-filled fractures located closer to the fault core. Some idiomorphic siderite rhombs are locally recognized in transmitted light or with BSE-SEM (Fig. 8). In some places, the dense siderite infill is cut by composite siderite–ankerite

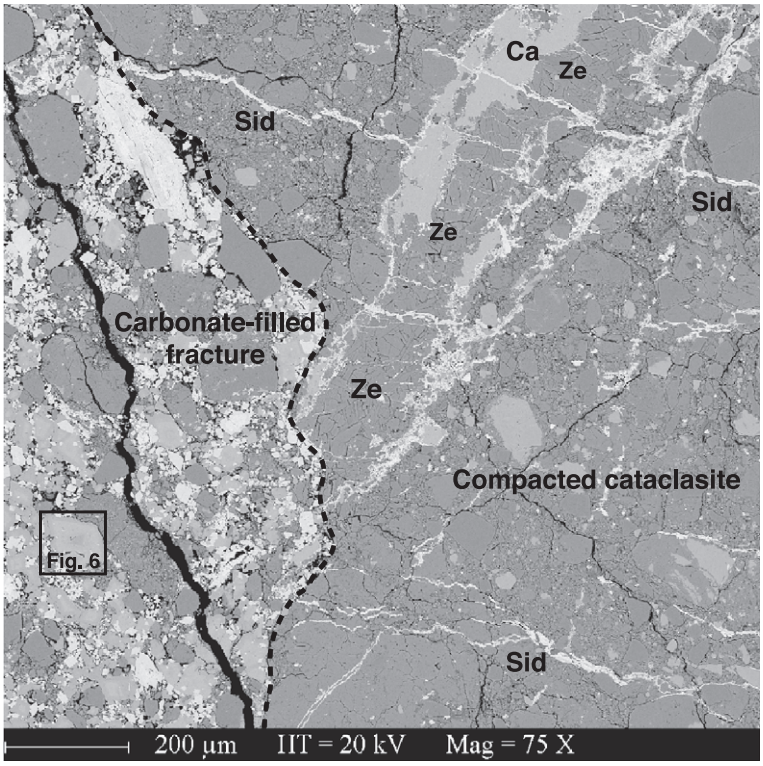

Fig. 4. BSE-SEM image of thin section HR2-48 in sample 098-31 showing the contact (discontinuous black line) between a carbonate-filled fracture on the left, and compacted cataclasite. The fracture cuts a grey zeolite vein (Ze), a light grey calcite vein (Ca), and white siderite veinlets (Sid) which are parallel or at high angle to the compaction plane of the cataclasite. Location of Fig. 6 is also shown.

veins showing a blocky to faceted (open-space filling) internal texture.

4. Chronology of structures

On the basis of cross-cutting relationships, the succession of deformation textures in the fault core from oldest to youngest is as follows (Tanaka et al., 2001; Fujimoto et al., 2001; Ohtani et al., 2000, 2001): pseudotachylites, cataclasites and ultracataclasites, zeolite veins, blocky carbonate veins, fibrous siderite veinlets parallel to the foliation, fine-grained carbonate-filled fractures, and very thin gouge zones. Therefore, most of the carbonate-filled fractures are not deformed and appear to be among the youngest deformation textures in the fault zone. However, some reworking of these veins has been locally observed in close vicinity to the fault in samples 098-29, 098-30 and 098-31 (Fig. 2d, e and f, respectively), which correspond approximately to a 12-cm-thick zone located above the fault plane. Two types of reworked textures can be recognized: (i) change in shape and compaction, and (ii) fracturing and attrition in thin gouge zones.

In the thin section HR2-48 (sample 098-31), both undeformed (see descriptions above) and compacted carbonate filling coexist. Two thin (50 μm) zones of very fine-grained (1–10 μm) gouge parallel to the main fault orientation cut sharply all of the previous deformation structures, carbonate-filled fractures included (Fig. 9). Between these two gouge zones, the carbonate grains display serrated grain boundaries and truncated oscillatory zonation due to indentation of original idiomorphic rhombs by particles of silicate fragments (Fig. 10). Some ankerite crystals are penetrated by smaller siderite ones, and one siderite crystal is indented by an illite

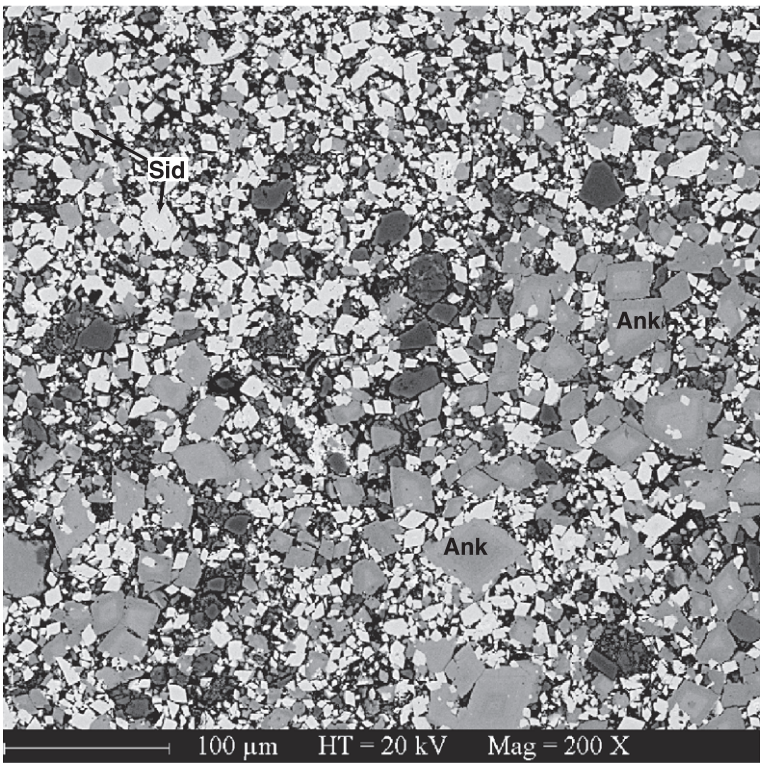

Fig. 5. BSE-SEM image of thin section HR2-48 in sample 098-31 showing a large fracture mostly filled by siderite rhombs (white) at the top and by ankerite (medium grey) plus siderite (white) rhombs at the bottom. Crystal size distribution has been determined on this BSE-SEM image.

flake (Fig. 10). The average flattening plane of the crystals is oblique to the orientation of the gouge zones. This relationship is indicative of an apparent reverse movement on these shear planes, which is compatible with the reverse dextral displacement on the Nojima fault during the Hyogo-ken Nanbu earthquake.

5. Composition of the carbonate crystals

The composition of the carbonate rhombs has been determined using electron microprobe and BSE-SEM. These techniques show that both types of rhombs are solid solutions combining the elements Ca, Mg, Fe and Mn in different proportions (Table 1).

These results confirms the ankeritic and sideritic nature of these carbonates by comparison with chemical analyses given by Chang et al. (1996). Both types of carbonate rhombs also contain a small quantity of Mn (up to 1.1% MnO, Table 1).

Analyses by BSE-SEM along a profile show the variations in Ca, Mg, Fe, and Mn concentrations within the ankerite rhombs (Fig. 6). These variations—higher Ca and Mg contents but lower Fe content—are consistent with the slightly darker rim of the ankerite rhombs on BSE-SEM images. Zonation of the siderite rhombs could not be studied because of their small size and due to interference from surrounding minerals.

6. Composition of the groundwater

The Hirabayashi borehole was completed with a casing that is perforated in the 630 and 650 m depth interval, just below the main fault plane within the

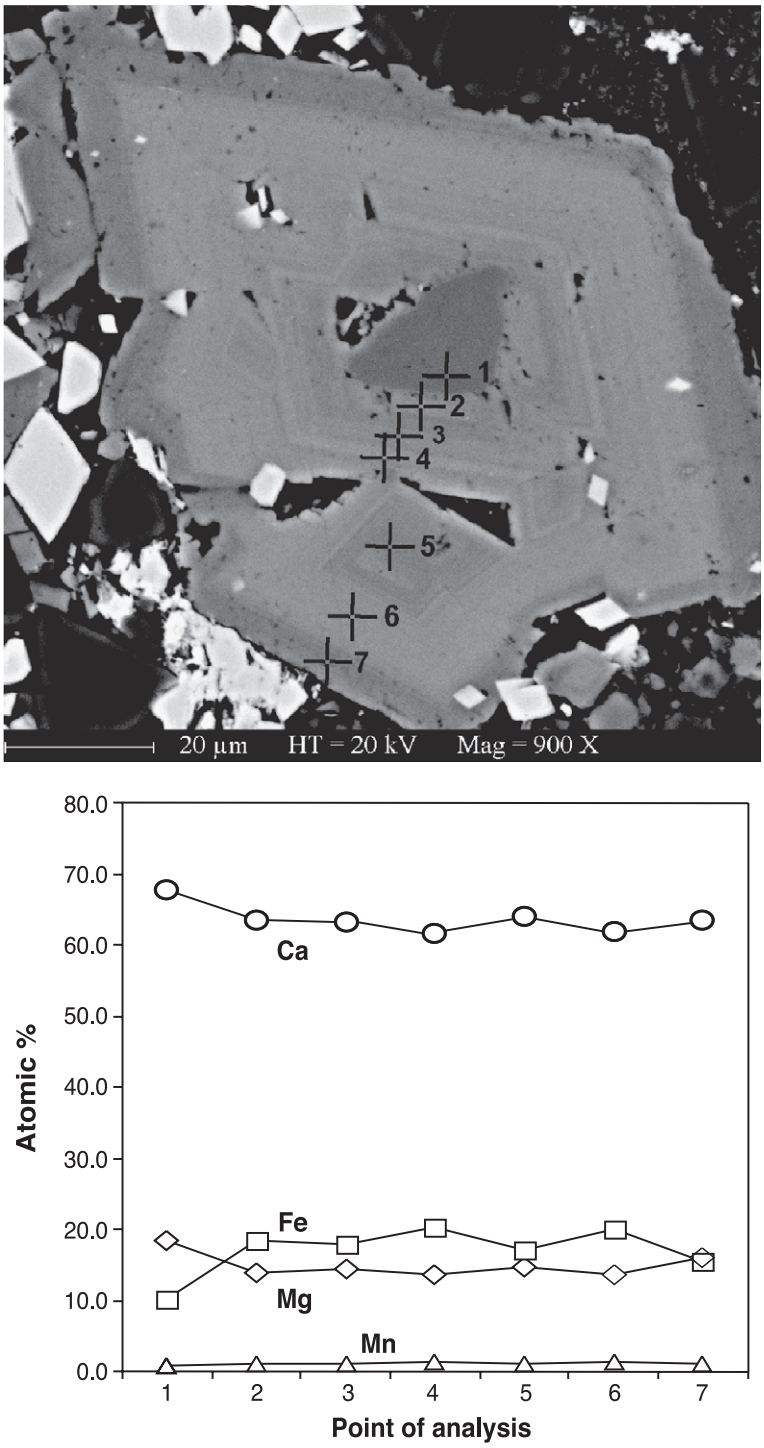

Fig. 6. BSE-SEM image of thin section HR2-48 in sample 098-31 of the ankerite rhomb located in the lower left corner of Fig. 4. Note that the rhomb is a composite crystal made of several agglomerated rhombs, and that some siderite crystals are included in the ankerite crystal. Analyses by BSE-SEM are located and reported below.

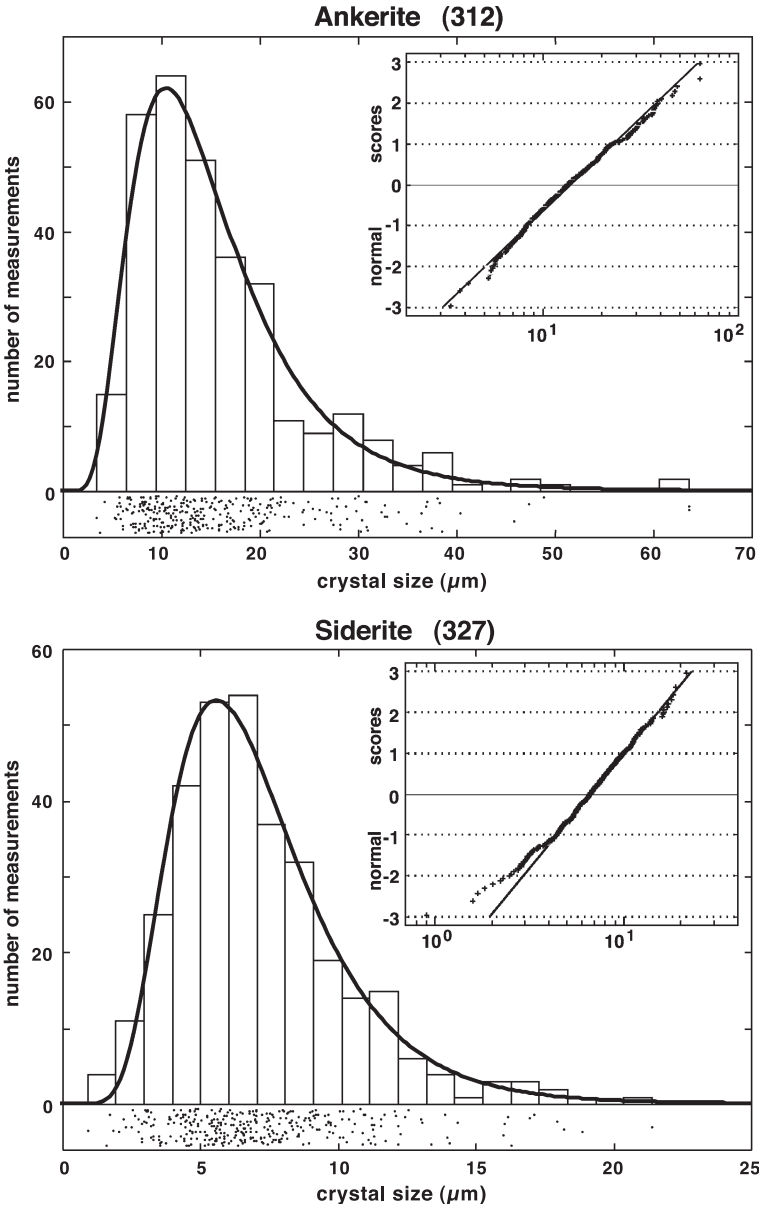

Fig. 7. Crystal size distributions for 317 ankerite and 327 siderite crystals as manually measured on the BSE-SEM image of Fig. 5. The major axes of crystals have been measured (NIH image program). Below each histogram, individual measurements are reported as dots. Two best-fitting log-normal distributions are also drawn (continuous curves) on the respective histograms for comparison. They have been determined through a simple fit in the "normal score" vs. "log of size" diagrams shown as insets; their respective parameters are: $\mu = 2.61$, $\sigma = 0.50$ for ankerite, and $\mu = 1.90$, $\sigma = 0.41$ for siderite.

footwall. Pumping tests were performed and the vertical hydraulic diffusivity was estimated to be 0.5 m^2/s (Roeloffs and Matsumoto, 1999). Water has been sampled in the borehole 1 year after the Hyogo-ken Nanbu earthquake in 1996 during the pumping test (pumping rate was 50 l/min).

Electric conductivity and pH were measured on-site with electrodes after sampling. The borehole

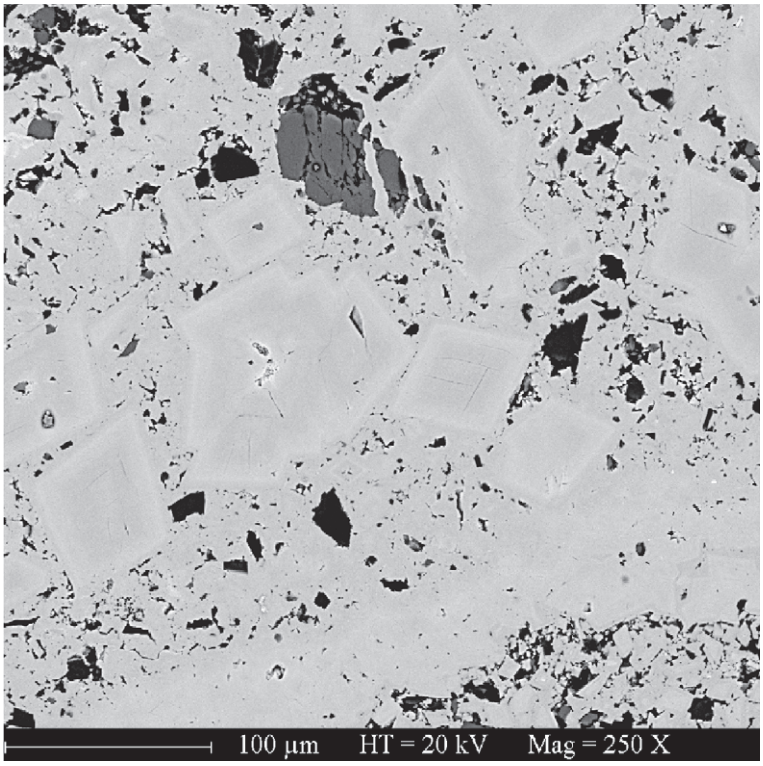

Fig. 8. BSE-SEM image of thin section HR2-8 in sample 094-10 (see Fig. 2a) showing zoned euhedral siderite rhombs within a fracture. Note that only a few voids remain and that almost the entire vein is cemented by siderite.

water was immediately filtered through a 0.45-µm membrane, acidified, and stored in plastic bottles for subsequent chemical analysis. The analyses were conducted by Mitsubishi Materials.

Total iron and Fe^{+3} were analyzed using spectrophotometric techniques. The samples were pretreated by addition of aliquots of 1,10-phenanthroline, HCl and ammonium acetate solutions for Fe^{+3} determinations. For total iron determinations, HCl, hydrochloric hydroxylamine solution, 1,10-phenanthroline and ammonium acetate solution were added to water samples. Ferrous ion was calculated from the difference between total iron and Fe^{+3}.

Titration method was used for carbonate species determinations. Anions were measured by ion chromatography and cations were determined by ICP-AES. Analytical uncertainties are typically about 5–10% for trace components and better than 5% for major components.

The chemical composition of the groundwater is shown in Table 2 (Sato and Takahashi, 1997, 1999). A gas-tight sampling apparatus was used in 1999 during other pumping tests. The chemistry (major ions and elements) was almost the same as the groundwater sampled during the 1996 pumping test (Fujimoto, unpublished data).

The geochemical speciation model PHREEQC-2 (Parkhurst and Appelo, 1999) was used to calculate the distribution of different ionic species in groundwater. PHREEQC-2 is based on an ion-association aqueous model and has capabilities for speciation and saturation index ($SI = \log_{10}(IAP/K_{sp})$) calculations (see http://www.brr.cr.usgs.gov/projects/GWC_coupled/phreeqc/index.html). The results of these calculations indicate that the present-day groundwater is at near equilibrium ($SI = 0$) or slightly oversaturated ($SI > 0$) with respect to aragonite ($SI = 0.5$), calcite (0.64), chalcedony (0.54), dolomite (1.18), quartz (0.95),

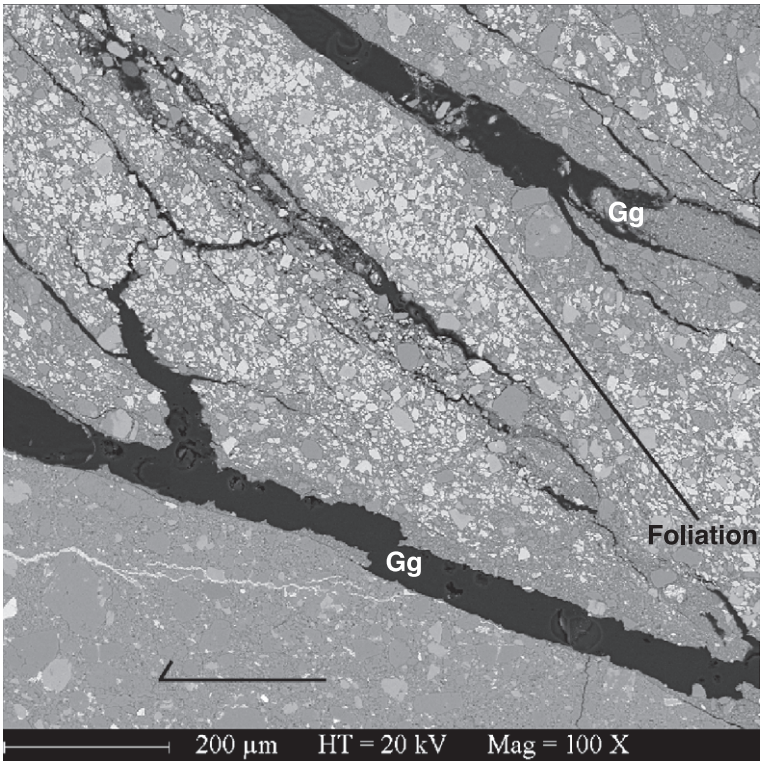

Fig. 9. BSE-SEM image of thin section HR2-48 in sample 098-31 (see Fig. 2f) showing a zone rich in carbonate rhombs and delimitated by two very thin gouge zones (Gg) in the upper right corner of Fig. 3a. The black arrow points to the top of the borehole. The flattening plane of the rhombs (solid black line) is oblique to the gouge zones, which are themselves parallel to the orientation of the main Nojima fault plane. This geometry is consistent with a reverse component on the gouge zones and is compatible with the last 1995 Hyogo-ken Nanbu earthquake.

rhodochrosite (0.29) and siderite (0.96), but is supersaturated to highly supersaturated with respect to amorphous iron hydroxide (2.88), goethite (8.77) and hematite (19.47). Some of these minerals (e.g., calcite, dolomite, siderite, rhodochrosite) are present as solid solutions in the carbonate rhombs, while others (e.g., quartz, clays) occur as very small wall-rock fragments in the carbonate-filled fractures or within the cataclasites as shown by X-ray diffraction analyses (Ohtani et al., 2000).

The SiO_2 content of the groundwater may be used also to calculate the reservoir temperature (Fournier, 1985). Our calculations suggest a temperature of 97 °C, with the reservoir situated at approximately 4 km depth using a geothermal gradient estimated to be 24 °C/km from the measurements of the thermal conductivity of drill core samples and the temperature logging data in the borehole (Kitajima et al., 1998; Yamaguchi et al., 1999).

7. Discussion and interpretation

The internal structures of the fractures and the idiomorphic shape of the carbonate rhombs suggest that numerous, small carbonate crystals grew in open spaces, nucleated almost simultaneously, and that significant subsequent growth has been limited and restricted to the ankerite rhombs. Nucleation and growth mechanisms may be discussed more precisely on the basis of the log-normal crystal size distributions of siderite and ankerite crystals which indicate that these crystals originated by decaying-rate nucleation accompanied by surface-controlled growth in a

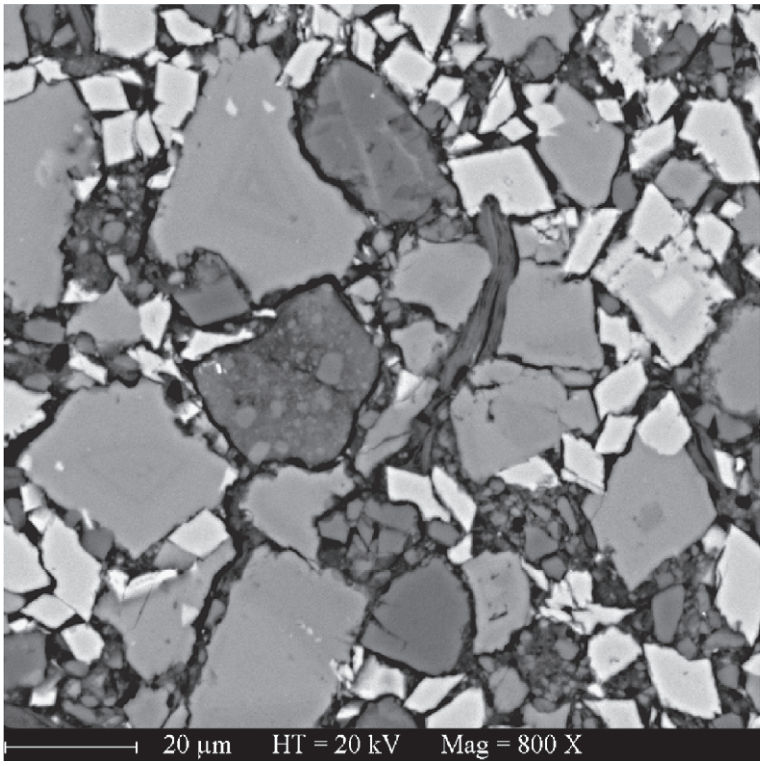

Fig. 10. BSE-SEM image of thin section HR2-48 in sample 098-31 (see Fig. 2f) showing details of the carbonate-rich compacted zone (see Fig. 3 for location). Siderite and ankerite rhombs show dissolution features due to indentation by harder particles, such as fragments of silicate minerals or ultracataclasites.

fluid saturated with respect to these carbonates (Kile et al., 2000). The slight departure of the two sets of measurements from a best-fitted theoretical log-normal distribution (Fig. 7) can be attributed to a statistical sampling effect. The similar shape (asymmetry and standard deviation over mean value ratio) of both distributions is interpreted in terms of similar nucleation and growth processes of ankerite and siderite.

Table 1
Oxides by weight percent of the carbonate rhombs measured with a Cameca SX100 electron probe and recalculated in terms of principal carbonate components

Sample (depth, m)	Point	Mineral	FeO	MnO	CaO	MgO	Total	$FeCO_3$	$MnCO_3$	$CaCO_3$	$MgCO_3$	Total
619.8	#12	siderite	49.67	1.10	2.98	7.06	60.81	81.69	1.81	4.89	11.61	100.00
619.8	#31	siderite	42.23	0.92	5.15	8.60	56.90	74.22	1.61	9.05	15.12	100.00
619.8	#13	ankerite	11.87	0.64	29.76	9.92	52.20	22.74	1.23	57.02	19.01	100.00
619.8	#32	ankerite	10.03	0.48	29.52	10.86	50.88	19.71	0.94	58.01	21.34	100.00
622.6	#51	siderite	47.20	0.88	2.97	6.79	57.84	81.61	1.52	5.13	11.73	100.00
622.6	#70	siderite	41.08	1.01	5.87	9.08	57.04	72.02	1.77	10.29	15.93	100.00
622.6	#72	siderite	43.53	0.89	3.23	11.46	59.11	73.65	1.51	5.46	19.39	100.00
622.6	#52	ankerite	9.31	0.47	31.42	11.98	53.18	17.51	0.88	59.08	22.53	100.00
622.6	#69	ankerite	12.34	0.69	31.51	10.29	54.83	22.50	1.26	57.48	18.76	100.00
622.6	#71	ankerite	12.26	0.68	32.22	9.60	54.76	22.39	1.24	58.84	17.54	100.00

Table 2
Chemical composition of the groundwater obtained from the Hirabayashi well (after Sato and Takahashi, 1999)

Temperature	pH	E.C.	HCO_3^-	CO_3^{2-}	Cl^-	SO_4^{2-}	NO_3^-	F^-	Br^-	Li^+	Na^+	K^+	Ca^{2+}	Mg^{2+}	Sr^{2+}	Mn^{2+}	Fe^{2+}	Fe^{3+}	CO_2	H_2S	H_2SiO_3	HBO_3	$HAsO_2$
23.9 °C	7.8	60.3 (ms/m)	330 (mg/l)	<5 (mg/l)	20.4 (mg/l)	5.1 (mg/l)	<0.05 (mg/l)	0.7 (mg/l)	0.09 (mg/l)	<0.1 (mg/l)	36.2 (mg/l)	4.7 (mg/l)	56.2 (mg/l)	20.0 (mg/l)	0.5 (mg/l)	0.16 (mg/l)	1.00 (mg/l)	0.94 (mg/l)	<0.001 (mg/l)	<0.001 (mg/l)	57.2 (mg/l)	1.20 (mg/l)	0.008 (mg/l)

The groundwater was sampled in the borehole 1 year after the Hyogo-ken Nanbu earthquake in 1996 during the pumping test. Details on analytical procedures are explained in the text.

The difference between mean values (and proportionally standard deviations) may be attributed to the chemistry of the solution.

Jimenez-Lopez et al. (2001) describe precipitation of calcite during experiments performed at 25 °C and 1 atm in a supersaturated solution. They first obtained small spherulites of monohydrocalcite which were progressively replaced in time by 15 μm crystals displaying the characteristic rhombohedral habit of calcite. After 300 min, which is a geologically short time frame, only well-faceted rhombohedra were detected. Thus, the carbonate filling of the fractures in the Nojima sample may have also precipitated very quickly in a supersaturated solution with respect to siderite and ankerite and at low temperature.

Siderite and ankerite are common minerals in sedimentary rocks. Morad (1998) proposes diagrams of temperature-dependent equilibrium relationships among the principal carbonates (calcite, ankerite, dolomite, magnesite, siderite) as functions of the ratios of the ionic activities of Ca^{2+}, Mg^{2+} and Fe^{2+} in groundwater. These activities have been calculated for the Hirabayashi groundwater and they fall within the stability field of siderite on $\log(a\mathrm{Fe}^{2+}/a\mathrm{Ca}^{2+})$ and $\log(a\mathrm{Fe}^{2+}/a\mathrm{Mg}^{2+})$ vs. temperature diagrams, and within the stability field of dolomite in the $\log(a\mathrm{Mg}^{2+}/a\mathrm{Ca}^{2+})$ vs. temperature diagram. As pointed out by Morad (1998), the precipitation conditions and equilibrium relationships of carbonate are controlled by several inter-related parameters such as water chemistry (ionic activities, pH, alkalinity), kinetics and temperature; equilibrium thermodynamics may not apply to precipitation processes in geological contexts where these parameters vary rapidly in time.

Solution supersaturation and precipitation of carbonates may have originated by a fluid pressure drop as already suggested by Eichhubl and Boles (2000). The same process has been invoked by Robert et al. (1996) for fine-grained gold-bearing quartz veins, by Herrington and Wilkinson (1993) for colloidal gold and silica in mesothermal vein systems, and by Coulon and Frizon de Lamotte (1988), Labaume et al. (1997), and Evans et al. (1998) for fine-grained carbonate fillings of hydraulic fractures in chalk, clays and sandstones, respectively. Such a fluid pressure drop may have been an immediate consequence of co-seismic hydraulic fracturing as proposed by Sibson et al. (1988) in

their fault-valve model and as suggested in the scenario of Fig. 11. Before an earthquake, the pore fluid pressure in cataclastic fault rocks may be higher than the hydrostatic value as a result of compaction and reduction of permeability by pressure solution (Gratier et al., 2003). Therefore, as soon as the earthquake occurs, fluid pressure drops to hydrostatic value due to fractures which form highly permeable channel ways for fluid flow (Sibson et al., 1988). The solubility of calcite in water strongly depends on the temperature (retrograde solubility), the partial pressure of CO_2, and pH. The lower the temperature, the greater the decrease in calcite solubility induced by a decrease in partial pressure of CO_2 (review in Fyfe et al., 1978). For example, a slight decrease in partial pressure of CO_2 (from 12 to 4 bar) at 100 °C is sufficient to induce a decrease of calcite solubility from 0.6 to 0.4 g $CaCO_3$/kg solution. Therefore, the fast ascent of a fluid from a 4 km depth at 100 °C to shallower levels would probably induce a strong decrease in partial pressure of CO_2, and in calcite solubility, and thus the nucleation and precipitation of numerous rhombs in open fractures.

After crystallization, the ankerite and siderite rhombs have suffered some deformation. The changes in crystal shapes in between the two gouge zones (Figs. 9, 10) are very similar to textures described in sandstones from subsiding sedimentary basins (Bjørkum, 1996; Renard et al., 1997). We interpret their textures as a result of pressure solution indentation of soluble crystals (ankerite and siderite) by less soluble particles (fragments of cataclasite, illite included). The carbonate crystals were also affected by brecciation or attrition in very thin low angle gouge zones (Figs. 9 and 11). Similar thin gouge zones are also observed below the main fault plane, at a 625–635 m depth interval. Indentation and compaction by pressure solution are low strain-rate processes occurring during the aseismic stage, and brecciation and attrition are

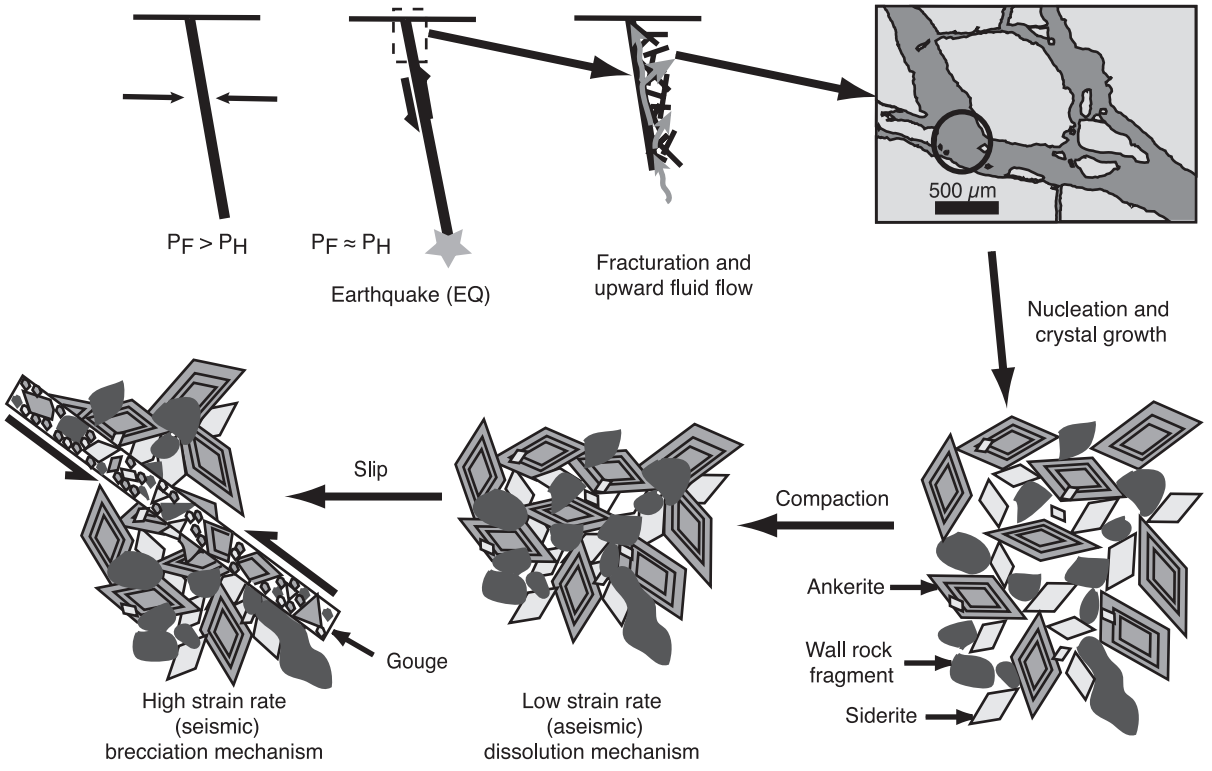

Fig. 11. Interpretative sketch depicting the formation of the carbonate-filled fractures and their subsequent evolution. Explanations in the text.

high strain-rate processes occurring during the seismic stage (Gratier and Gamond, 1990). The width of the gouge zones (<1 mm) suggests that the corresponding seismic events were of low magnitude, although there is no established scale relationship between the thickness of the seismic slip zones and the magnitude of the seismic events due to localisation of co-seismic shearing (Sibson, 2003). As the carbonate fractures have probably formed at low temperatures and shallow depths, the narrow gouge zones are probably also the expression of shallow slip zones. We may constrain the maximum depth of formation of both the carbonate veins and the thin gouge zones when considering the recent 490–540 m vertical offset of the Kobe Group on the Nojima fault plane and the 625 m depth where these textures are actually observed. Therefore, they probably formed at a depth less than 1100 m.

Very finely crystallized veins are rarely described in the literature and we believe that they may represent transient geological microstructures (see Robert et al., 1996; Herrington and Wilkinson, 1993; Coulon and Frizon de Lamotte, 1988; Labaume et al., 1997; Evans et al., 1998). These fine-grained veins may later become entirely recrystallized due to the action of circulating fluids; this is probably the case of the siderite veins observed in other sections of the Hirabayahi borehole (see Figs. 2a and 8) where all the void spaces between wall-rock fragments have been filled by siderite. On the other hand, these microstructures may dissolve via a pressure-solution process, as described in sample 098-31 (Fig. 2f), and thereby making their observation impossible. Therefore, only observation of very young faults and associated veins may allow for the observation of transient, primary fine-grained textures.

8. Conclusions

We have shown that co-seismic hydraulic fracturing occurred in the hanging wall of the Nojima fault, as evidenced by the distribution of carbonate fractures on an approximately 1-m-thick zone above the fault plane. These fractures are filled by small euhedral ankerite and siderite crystals that have been interpreted as having been derived from decaying-rate nucleation and surface-controlled growth in a supersaturated fluid with respect to these carbonates. A slight decrease in fluid or CO_2 partial pressure may have been the cause of the carbonate oversaturation of the circulating fluid, which could have been similar in composition to the present-day groundwater sampled in the borehole.

The carbonate fractures occur very late in the evolution of the Nojima fault but do not represent the last event since they are cut by thin gouge zones and have been subjected to pressure solution processes. They have suffered at least one seismic cycle represented by low strain-rate deformation (pressure solution) during the interseismic stage, and high strain-rate deformation (slip in gouge zones) during the subsequent seismic stage. These carbonate fractures seems to be present only above the fault plane and, therefore, are consistent with preferential fluid circulation and intense alteration within the hanging wall, as observed by Ohtani et al. (2000).

Internal textures of veins or fractures displaying fine-grained euhedral crystals are rarely described in the literature and this may be explained by their transient nature subject to rapid modification by recrystallization or by dissolution–precipitation processes.

In conclusion, the drilling of active faults gives scientists the opportunity to observe transient textures due to recent earthquakes, which otherwise are impossible to observe on exhumed faults, and to integrate and combine all of the textural, mineralogical, and chemical data with logging measurements so as to yield a real-time snapshot of the fault.

Acknowledgements

The authors thank D. Mainprice, R. Hellmann, S.M.F. Sheppard and R.H. Sibson for discussions and for their interest on the textures of the Nojima fault rocks. They acknowledge T. Nogami and C. Nevado for making high quality thin sections, and S. Pairis and C. Merlet for technical support using the SEM and electron microprobe. They are grateful to Cornel de Ronde, an anonymous reviewer and Christopher Wibberley for their constructive comments and their helpful suggestions during the review of the manuscript.

References

Awata, Y., Mizuno, K., 1997. Strip map of the surface fault ruptures associated with the 1995 Hyogo-ken Nanbu earthquake, central Japan—the Nojima, Ogura and Nadagawa earthquake faults. Geological Survey of Japan, Tsukuba, 74 pp. (in Japanese with English abstract).

Bjørkum, P., 1996. How important is pressure in causing dissolution of quartz in sandstones? Journal of Sedimentary Research 66 (1), 147–154.

Bons, P.D., 2000. The formation of veins and their microstructures. In: Jessell, M.W., Urai, J.L. (Eds.), Stress, Strain and Structure, A volume in honour of W.D. Means. Journal of Virtual Explorer, vol. 2. ISSN 1441-8126 (on line at www.virtualexplorer.com.au/VEjournal/Volume2).

Boullier, A.M., Ohtani, T., Fujimoto, K., Ito, H., Dubois, M., 2001. Fluid inclusions in pseudotachylytes from the Nojima fault Japan. Journal of Geophysical Research 106 (B10), 21965–21977.

Caine, J., Evans, J., Forster, C., 1996. Fault zone architecture and permeability structure. Geology 26 (11), 1025–1028.

Chang, L.L.Y., Howie, R.A., Zussman, J., 1996. Non-silicates: sulphates, carbonates, phosphates, halides. Rock-Forming Minerals, 5B. Longman Group, London, UK. 383 pp.

Coulon, M., Frizon de Lamotte, D., 1988. Les craies éclatées du secteur d'Omey (Marne, France): le résultat d'une bréchification par fracturation hydraulique en contexte extensif. Bulletin de la Société géologique de France IV (8), 177–185.

Cox, S.F., 1995. Faulting processes at high fluid pressures: an example of fault valve behavior from the Wattle Gully Fault Victoria, Australia. Journal of Geophysical Research 100 (B7), 12841–12859.

de Ronde, C.E.J., Sibson, R.H., Bray, C.J., Faure, K., 2001. Fluid chemistry of veining associated with an ancient microearthquake swarm, benmore Dam, New Zealand. Geological Society of America Bulletin 113 (8), 1010–1024.

Eichhubl, P., Boles, J.R., 2000. Rates of fluid flow in fault systems—evidence for episodic rapid fluid flow in the Miocene Monterey Formation, coastal California. American Journal of Science 300, 571–600.

Evans, R., Hendry, J.P., Parnell, J., Kalin, R.M., 1998. Origin and significance of fracture-related dolomite in porous sandstones: an example from the Carboniferous of County Antrim, Northern Ireland. In: Morad, S. (Ed.), Carbonate cementation in sandstones Special Publication of the International Association of Sedimentologists, vol. 26. Blackwell Science, Oxford, UK, pp. 409–435.

Fournier, R.O., 1985. The behaviour of silica in hydrothermal solutions. Reviews in Economic Geology 2, 45–62.

Fujimoto, K., Tanaka, H., Higuchi, T., Tomida, N., Ohtani, T., Ito, H., 2001. Alteration and mass transfer inferred from the Hirabayashi GSJ drill core penetrating the Nojima Fault Japan. The Island Arc 10 (3–4), 401–410.

Fyfe, W.S., Price, N.J., Thompson, A.B., 1978. Fluids in the Earth's crust. Elsevier, Amsterdam. 383 pp.

Gratier, J.P., Gamond, J.F., 1990. Transition between seismic and aseismic deformation in the upper crust. In: Knipe, R.J., Rutter, E.H. (Eds.), Deformation Mechanisms, Rheology and Tectonics, vol. 54. Geological Society Special Publication, Bath, UK, pp. 461–473.

Gratier, J.P., Favreau, P., Renard, F., 2003. Modeling fluid transfer along California faults when integrating pressure solution crack sealing and compaction processes. Journal of Geophysical Research 108 (B2), 2104. doi: 10.1029/2001JB000380.

Herrington, R.J., Wilkinson, J.J., 1993. Colloidal gold, silica in mesothermal vein systems. Geology 21, 539–542.

Hickman, S., Sibson, R.H., Bruhn, R., 1995. Introduction to special section: mechanical involvement of fluids in faulting. Journal of Geophysical Research 100 (B7), 12831–12840.

Ito, H., Kuwahara, Y., Miyazaki, T., Nishizawa, O., Kiguchi, T., Fujimoto, K., Ohtani, T., Tanaka, H., Higuchi, T., Agar, S., Brie, A., Yamamoto, H., 1996. Structure and physical properties of the Nojima Fault. BUTSURI-TANSA (Geophysical Exploration) 49, 522–535 (in Japanese with English abstract).

Jimenez-Lopez, C., Caballero, E., Huertas, F.J., Romanek, C.S., 2001. Chemical, mineralogical and isotope behavior, and phase transformation during the precipitation of calcium carbonate minerals from intermediate ionic solution at 25 °C. Geochimica et Cosmochimica Acta 65, 3219–3231.

Kile, D.E., Eberi, D.D., Hoch, A.R., Reddy, M.M., 2000. An assessment of calcite crystal growth mechanisms based on crystal size distributions. Geochimica et Cosmochimica Acta 64 (17), 2937–2950.

Kitajima, T., Kobayashi, Y., Ikeda, R., Iio, Y., Omura, K., 1998. Terrestrial heat flow in Nojima–Hirabayashi, Awaji Island. Chikyu Monthly 21, 108–113 (in Japanese).

Labaume, P., Kastner, M., Travé, A., Henry, P., 1997. Carbonate veins from the décollement zone at the toe of the northern Barbados accretionary prism (ODP Leg 156): relationships with structures and fluid regime. Proceedings of the Ocean Drilling Program, Scientific Results: College Station, TX (Ocean Drilling Program) 156, 79–96.

Morad, S., 1998. Carbonate cementation in sandstones: distribution patterns and geochemical evolution. In: Morad, S. (Ed.), Carbonate cementation in sandstones Special Publication of the International Association of Sedimentologists, vol. 26. Blackwell Science, Oxford, UK, pp. 1–26.

Muir-Wood, R., King, G., 1993. Hydrological signatures of earthquakes strain. Journal of Geophysical Research 98 (B12), 22035–22068.

Murata, A., Takelmura, K., Miyata, T., Lin, A., 2001. Quaternary vertical offset and average slip rate of the Nojima Fault on Awaji Island, Japan. Island Arc 10, 360–367.

Ohtani, T., Fujimoto, K., Ito, H., Tanaka, H., Tomida, N., Higuchi, T., 2000. Fault rocks and past to recent fluid characteristics from the borehole survey of the Nojima fault ruptured in the 1995 Kobe earthquake, southwest Japan. Journal of Geophysical Research 105 (B7), 16161–16171.

Ohtani, T., Tanaka, H., Fujimoto, K., Higuchi, T., Tomida, N., Ito, H., 2001. Internal structure of the Nojima Fault Zone from the Hirabayashi GSJ drill core. The Island Arc 10, 392–400.

Parkhurst, D.L., Appelo, C.A.J., 1999. PHREEQC (Version 2), A computer program for speciation, batch-reaction, one-dimensional transport and Inverse geochemical calculations. Water-

Resources Investigations Report 99-4259, U.S. Geological Survey, Denver, CO.

Renard, F., Ortoleva, P., Gratier, J.P., 1997. Pressure solution in sandstones: influence of clays and dependence on temperature and stress. Tectonophysics 280, 257–266.

Robert, F., Boullier, A.M., Firdaous, K., 1995. Gold-quartz veins in metamorphic terranes and their bearing on the role of fluids in faulting. Journal of Geophysical Research 100 (B7), 12861–12879.

Robert, F., Boullier, A.M., Firdaous, K., 1996. Geometric aspects of a large extensional vein Donalda deposit, Rouyn-Noranda, Quebec. Current Research-Geological Survey of Canada, 1996-C, 147–155.

Roeloffs, E., Matsumoto, N., 1999. Changes of water level and stress condition around Nojima fault. In: Ito, H., Fujimoto, K., Tanaka, H., Lockner, D. (Eds.), International Workshop of the Nojima Fault Core and Borehole Data Analysis. Geological Survey of Japan, Tsukuba, Japan, pp. 173–177.

Sato, T., Takahashi, M., 1997. Geochemical changes in anomalously discharged groundwater in Awaji Island after the 1995 Kobe earthquake. Chikyukagaku 31, 89–98 (in Japanese with English abstract).

Sato, T., Takahashi, M., 1999. Chemical and isotopic compositions of groundwater obtained from the Hirabayashi well. In: Ito, H., Fujimoto, K., Tanaka, H., Lockner, D. (Eds.), International workshop of the Nojima fault core and borehole data analysis. Geological Survey of Japan, Tsukuba, Japan, pp. 187–192.

Secor, D.T., 1965. Role of fluid pressure in jointing. American Journal of Science 263, 633–646.

Sibson, R.H., 2003. Thickness of the seismic slip zone. Bulletin of the Seismological Society of America 93, 1169–1178.

Sibson, R.H., Scott, J., 1998. Stress/fault control on the containment and release of overpressured fluids: examples from gold-quartz vein systems in Juneau, Alaska; Victoria, Australia and Otago, New Zealand. Ore Geology Reviews 13, 293–306.

Sibson, R.H., Robert, F., Poulsen, K.H., 1988. High angle reverse fault, fluid-pressure cycling and mesothermal gold quartz deposits. Geology 16, 551–555.

Tanaka, H., Fujimoto, K., Ohtani, T., Ito, H., 2001. Structural and chemical characterization of shear zones in the freshly activated Nojima fault, Awaji Island, southwest Japan. Journal of Geophysical Research 106 (B5), 8789–8810.

Tsunogai, U., Wakita, H., 1995. Precursory chemical changes in ground water: Kobe earthquake, Japan. Science 269, 61–63.

Yamaguchi, T., Yamano, M., Nagao, T., Goto, S., 1999. Temperature monitoring in a borehole drilled into the Nojima fault and radioactive heat production of core samples. In: Ito, H., Fujimoto, K., Tanaka, H., Lockner, D. (Eds.), International workshop of the Nojima fault core and borehole data analysis. Geological Survey of Japan, Tsukuba, Japan, pp. 277–282.

Yamamoto, Y., Kurita, H., Matsubara, T., 2000. Eocene calcareous nannofossils and dinoflagellate cysts from the Iwaya Formation in Awajishima Island, Hyogo Prefecture, southwest Japan, and their geologic implications. Journal of the Geological Society of Japan 106 (5), 379–382.